Subcarrier Index-Power Modulated Optical OFDM With Superposition Multiplexing for IMDD Transmission Systems

Chen, Lin; Al Halabi, Fadi; Giddings, Roger; Tang, Jianming

Journal of Lightwave Technology

DOI:
10.1109/JLT.2016.2617781

Published: 12/11/2016

Peer reviewed version

Subcarrier Index-Power Modulated Optical OFDM with Superposition Multiplexing for IMDD Transmission Systems

L. Chen, F. Halabi, R. P. Giddings, and J. M. Tang

***Abstract*—A novel signal transmission technique termed subcarrier index-power modulated optical OFDM with superposition multiplexing (SIPM-OOFDM-SPM) is proposed and investigated, for the first time, in which SIPM automatically creates an information-carrying subcarrier power pattern via assigning a high (low) signal modulation format to a high (low) power subcarrier, whilst SPM passively adds different signal modulation format-encoded complex numbers and assigns the sum to a high power subcarrier. In comparison with conventional OOFDM, SIPM and SPM enable extra information to be conveyed in both the new subcarrier index-power dimension and the conventional subcarrier-information-carrying dimension. In this paper, extensive numerical explorations of SIPM-OOFDM-SPM performance characteristics are undertaken, based on which optimum transceiver design parameters are identified. For IMDD PON systems, it is shown that SIPM-OOFDM-SPM considerably improves the signal transmission capacity, link power budget and system performance tolerances to both chromatic dispersion and fiber nonlinearity.**

***Index Terms*—Orthogonal frequency division multiplexing, coding and decoding, digital signal processing and passive optical networks.**

I. Introduction

With the exponential data traffic growth associated with unprecedented emerging bandwidth-hungry network applications and services, recent years have seen extensive research interests in utilizing commercially available 10G-class optics to achieve 25Gb/s/λ intensity-modulation and direct-detection (IMDD) passive optical networks (PONs) equipped with desirable software defined networking (SDN) functionalities such as reconfigurability, flexibility, scalability and elasticity [1]-[3]. To deliver such a challenging task in a cost-effective approach, optical orthogonal frequency division multiplexing (OOFDM) is regarded as a promising candidate [4] because of its high spectral efficiency and inherent digital signal processing (DSP) richness. In addition, OOFDM also offers a number of other unique signal transmission and networking features including, for example, automatic awareness of channel spectral characteristics, excellent adaptability to component/system/network imperfections, dynamically variable transmission capacity versus reach performance, and DSP-enabled transceiver functionalities of on-line channel multiplexing/demultiplexing in the digital domain [5].

It is well known [6],[7] that, to further improve the OOFDM transmission capacity and corresponding spectral efficiency for applications in the 10G-class optics-based IMDD PON systems, high-order signal modulation formats have to be applied, which, however, bring about the following two considerable drawbacks: a) quick complexity growths in DSP algorithms and transceiver architecture, and b) strong requirements in optical signal-to-noise ratio (OSNR). Inevitably this results in a degraded link power budget and an increased transceiver cost. To avoid these unwanted drawbacks, it is highly advantageous if extra information-bearing dimensions of the OOFDM technique can be exploited to considerably enhance its transmission capacity and corresponding spectral efficiency without compromising either the transceiver DSP/architecture complexity or minimum signal OSNR required for achieving a specific bit error rate (BER).

To introduce an extra information-bearing dimension to the conventional OFDM technique, for wireless Rayleigh fading channels, subcarrier-index modulated OFDM (SIM-OFDM) [8] has been reported, in which each individual quadrature amplitude modulation (QAM)-encoded subcarrier is activated or deactivated according to an incoming pseudo-random binary sequence (PRBS) stream, thus the resulting on-and-off subcarrier pattern within an OFDM symbol can be used as an extra dimension to convey user information. However, the incorrect detection of a subcarrier power status at the SIM-OFDM receiver causes the strong error propagation effect, which can, fortunately, be reduced by enhanced subcarrier-index modulation OFDM (ESIM-OFDM) proposed recently [9]. In ESIM-OFDM, each bit carried in the extra information-bearing dimension is encoded using a combined power status of two consecutive subcarriers.

Furthermore, also inspired by the underlying idea of SIM, OFDM with index modulation (OFDM-IM) [10] has also been

Manuscript received May 22, 2016. This work was supported by in part The Ser Cymru National Research Network in Advanced Engineering and Materials (NRN024 and NRN147), and in part by The Innovative UK TEROPON project.

L. Chen is with the College of Electronics and Information Engineering, Shanghai University of Electric Power, Shanghai, 200090, China. L. Chen is also with the School of Electronic Engineering, Bangor University, Bangor, LL57 1UT, UK. (e-mail: l.chen@bangor.ac.uk)

F. Halabi, R.P. Giddings and J.M. Tang are with the School of Electronic Engineering, Bangor University, Bangor, LL57 1UT, UK. (e-mails: eep604@bangor.ac.uk; r.p.giddings@bangor.ac.uk; and j.tang@bangor.ac.uk).

published very recently by making use of a maximum likelihood (ML) detector in the OFDM-IM receiver to determine the most likely active subcarriers. However, the DSP complexity of the ML detector grows exponentially with increasing the number of subcarriers, this causes serious difficulties in implementing the OFDM-IM technique in cost-sensitive and high-speed application scenarios. Here it should be pointed out, in particular, that in all the aforementioned techniques namely SIM-OFDM, ESIM-OFDM and OFDM-IM, only active subcarriers are capable of conveying QAM-encoded information, their overall signal transmission capacities and corresponding spectral efficiencies are, therefore, almost halved compared to conventional OFDM encoded using identical signal modulation formats.

To address such a challenge and further explore its feasibility for use in IMDD PON scenarios, more recently a new transmission technique termed subcarrier index-power modulated optical OFDM (SIPM-OOFDM) has been proposed [11],[12], in which a combination of both the subcarrier index and subcarrier power acts as an extra information-carrying dimension, where low and high power subcarriers are encoded using quadrature phase shift keying (QPSK) and 8-phase shift keying (8-PSK), respectively. More specifically, when a "1" ("0") bit of an incoming PRBS stream is encountered, the corresponding subcarrier is set at a high (low) power level and subsequently encoded using 8-PSK (QPSK) by truncating following 3 (2) bits from the input PRBS stream. Therefore, the resulting high and low subcarrier power pattern within an OFDM symbol can be used as an extra information-carrying dimension with all the subcarriers being activated. As a direct result, without increasing minimum required OSNR and degrading system tolerances to chromatic dispersion and fiber nonlinearity, SIPM-OOFDM exceeds the 8-PSK-encoded OOFDM signal bit rate by approximately 17%, and almost doubles the signal bit rate and corresponding spectral efficiency associated with 8-PSK-encoded SIM-OFDM, ESIM-OFDM and OFDM-IM.

As a significant extension to the authors' precious work [11],[12], the present paper introduces, for the first time, superposition multiplexing (SPM) (also called non-orthogonal multiple access in radio access networks [13]) into SIPM-OOFDM, this leads to the proposition of a novel transmission technique, referred to as SIPM-OOFDM with SPM (SIPM-OOFDM-SPM). Compared to SIPM-OOFDM, for a high power subcarrier, SPM is employed to passively add two 8-PSK- and QPSK-encoded complex numbers, and the resulting sum is assigned to the high power subcarrier. Whilst for a low power subcarrier, similar to SIPM-OOFDM, only a single QPSK-encoded complex number is assigned to the subcarrier. Clearly, SIPM-OOFDM-SPM enables more effective usage of all high power subcarriers. In the SIPM-OOFDM-SPM receiver, instead of utilizing a sophisticated successive interference cancellation algorithm [14],[15], a simple DSP algorithm presented in Section II is sufficient to recover the information conveyed by SPM-based high power subcarriers.

For IMDD PON systems of interest of the present paper, it is shown that SIPM-OOFDM-SPM enables a 28.6% signal transmission capacity improvement compared to SIPM-OOFDM using the same signal modulation formats. In addition, in comparison with 32-PSK/QPSK-encoded SIPM-OOFDM capable of offering a signal transmission capacity identical to 8-PSK/QPSK-encoded SIPM-OOFDM-SPM, the proposed technique reduces the minimum required signal OSNR, and simultaneously improves the system tolerances to both chromatic dispersion and Kerr effect-related fiber nonlinearity.

The rest of the paper is organized as followings: In Section II, detailed descriptions of the SIPM-OOFDM-SPM operating principle are presented with special attention being focused on subcarrier bit and power allocation/recovery, information encoding and decoding, as well as subcarrier power threshold calculations. In Section III, to maximize the achievable SIPM-OOFDM-SPM transmission performance, a set of optimum transceiver parameters are numerically identified, based on which extensive explorations of achievable transmission performances of SIPM-OOFDM-SPM IMDD PON systems are undertaken in terms of signal transmission capacity, BER performance, chromatic dispersion tolerance and Kerr effect-related fiber nonlinearity tolerance. Finally, the paper is summarized in Section V.

II. SIPM-OOFDM-SPM Operating Principle and Transceiver Architecture

As illustrated in Fig.1, the SIPM-OOFDM-SPM operating principle is similar to previously reported SIPM-OOFDM [11],[12], except that considerable modifications are made to relevant transceiver DSP functions that deal with bit allocation/recovery in the newly introduced information-bearing dimension and the conventional subcarrier-information-carrying dimension.

Fig. 1(a) shows the SIPM-OOFDM-SPM transmitter DSP procedures of how to allocate an information bit in the subcarrier index-power dimension and how to subsequently encode information bits in the conventional subcarrier-information-carrying dimension. As an example, for an incoming PRBS stream, when a "1" bit is encountered, firstly the corresponding subcarrier is set at a high power level, and then following 5 bits from the PRBS stream are truncated, of which the first 3 bits are encoded using 8-PSK, and the remaining 2 bits are encoded using QPSK. After that, these two 8-PSK- and QPSK-encoded complex numbers are passively added together. Such an addition operation is referred to as SPM. Finally the resulting complex number is assigned to the high power subcarrier, as seen in Fig.1(b). Whilst when a "0" bit is encountered, the corresponding subcarrier is taken at a low power level, and following 2 bits of the PRBS stream are encoded using QPSK. The QPSK-encoded complex number is assigned to the low power subcarrier, as shown in Fig.1(a) and Fig.1(b).

From the above description, it is easy to understand the following four aspects: i) a high (low) power subcarrier is capable of conveying 6(3) information bits in total; ii) The power of a subcarrier encoded using M-ary QAM ($M \geq 8$) varies

because of the random occurrence of various constellation points having different powers, therefore only signal modulation formats with circular constellations can be superposed by SPM; iii) The average power of a SIPM-OOFDM-SPM signal at symbol level varies from symbol to symbol. The similar behavior also occurs for conventional OOFDM encoded using M-ary QAM (M⩾8). Our extensive experimental demonstrations of end-to-end real-time OOFDM transmission systems have indicated that commercially-available optical and electrical components are capable of copping with such symbol-level power variations [16,17]; and iv) For a high power subcarrier, 8-PSK- and QPSK-encoding-based SPM operation produces four information-carrying satellite constellation points surrounding each virtual 8-PSK constellation point, as shown in Fig.1(c). This gives rise to total 32 information-carrying satellite constellation points, each of which represents a specific combination of a virtual 8-PSK constellation point and a virtual QPSK constellation point. This feature implies that 8-PSK- and QPSK-encoded SIPM-OOFDM-SPM supports a signal transmission capacity identical to SIPM-OOFDM encoded using 32-PSK and QPSK. The low-order signal modulation formats employed in SIPM-OOFDM-SPM increase the minimum Euclidean distance, thus resulting in a number of performance advantages over SIPM-OOFDM, as discussed in detail in Section IV.

In the receiver, after fast Fourier transform (FFT) and standard training sequence-based channel estimation and channel equalization, the subcarrier power threshold, $P_{threshold}$, which distinguishes the received power of each individual subcarrier between the predefined low level and high level, can be calculated using the formula expressed below:

$$P_{threshold} = \frac{min\left(P_{8PSK+QPSK}\right) + P_{QPSK}}{2} \quad (1)$$

where $P_{8PSK+QPSK}$ and P_{QPSK} are the received high and low subcarrier powers after equalization. It can be seen in Fig.1(c) that, as a direct result of the SPM operation, $P_{8PSK+QPSK}$ varies slightly from subcarrier to subcarrier and from symbol to symbol. To sufficiently enlarge the difference between $P_{8PSK+QPSK}$ and P_{QPSK}, minimum $P_{8PSK+QPSK}$ values are thus considered in Eq.(1). In addition, to effectively reduce the impact of random noises on $P_{threshold}$, the subcarrier power threshold is averaged periodically over time.

If the received power level of an information-bearing subcarrier is above (below), $P_{threshold}$, a "1" ("0") information bit carried in the subcarrier index-power dimension is thus recovered, and the information conveyed in the conventional subcarrier-information-carrying dimension can also be decoded using the approach presented below. It should also be noted that a wrong subcarrier power decision causes errors to occur in both the subcarrier index-power dimension and the conventional subcarrier-information-carrying dimension. Such errors, however, do not propagate across different subcarriers and symbols.

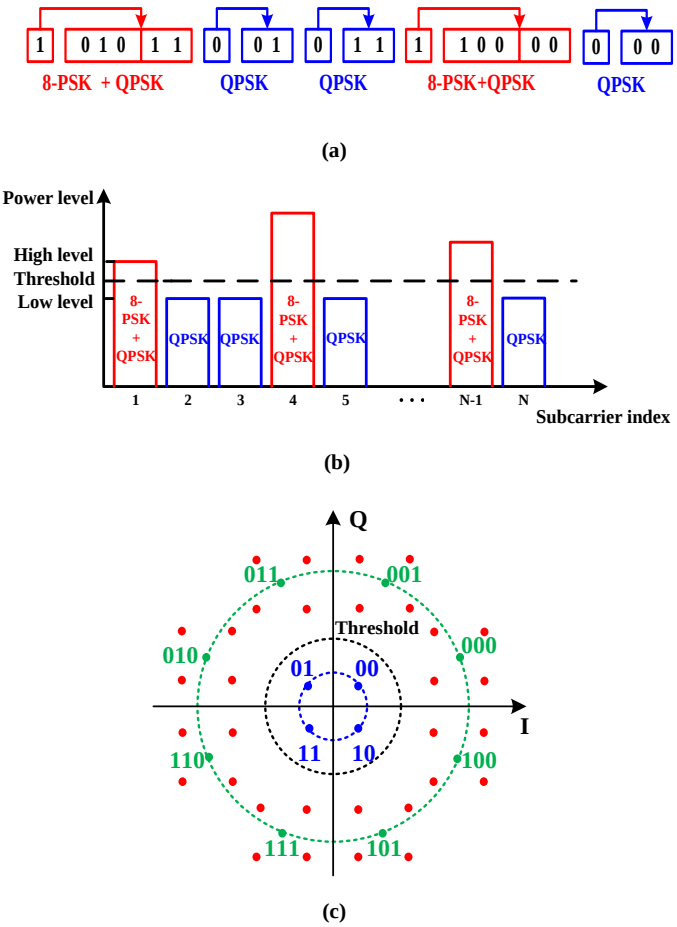

Fig. 1. (a) Bit allocations in the subcarrier index-power dimension and corresponding bit-encoding for both low and high power subcarriers in the conventional subcarrier-information-carrying dimension, (b) Subcarrier power allocations and 8-PSK- and QPSK-encoding-based SPM operation for high power subcarriers, and (c) overall SIPM-OOFDM-SPM constellations for high and low power subcarriers.

As the DSP process adopted for decoding low power subcarriers in the conventional subcarrier-information-carrying dimension is identical to that used in SIPM-OOFDM [11],[12], here attention is thus focused on the high power subcarrier decoding process. For a high power subcarrier, the received complex value after equalization can be written as:

$$C_R^E = C_4^* + C_8^* + \Delta C_4 + \Delta C_8 \quad (2)$$

where C_4^* and C_8^* represent the ideal "to be recovered" constellation points for QPSK and 8-PSK, respectively. ΔC_4 and ΔC_8 represent the differences between their actually received constellation point and their ideal constellation point. ΔC_4 and ΔC_8 arise due to the following three physical mechanisms including channel noise, nonlinear coupling, and channel frequency response. To recover the information carried by each high power subcarrier in the conventional subcarrier-information-carrying dimension, 32 comparisons

between C_R^E and all 32 possible combinations of ideal "to be recovered" C_{4i}^* (i=1,2,⋯,4) and ideal "to be recovered" C_{8j}^* (j=1,2,⋯,8) are made, of which the combination that gives rise to a minimum $\left|\Delta C_4 + \Delta C_8\right|^2$ is regarded as the information conveyed by the high power subcarrier in the conventional subcarrier-information-carrying dimension. The above description suggests that SIPM-OOFDM-SPM increases the de-mapping function complexity by a factor of approximately 2.5 in comparison with conventional 32-QAM-encoded OOFDM. However, the FPGA logic resource consumed by each of these two de-mapping functions is almost negligible compared to the total FPGA logic resource consumed by all DSP functions embedded in the transmitter or receiver [16].

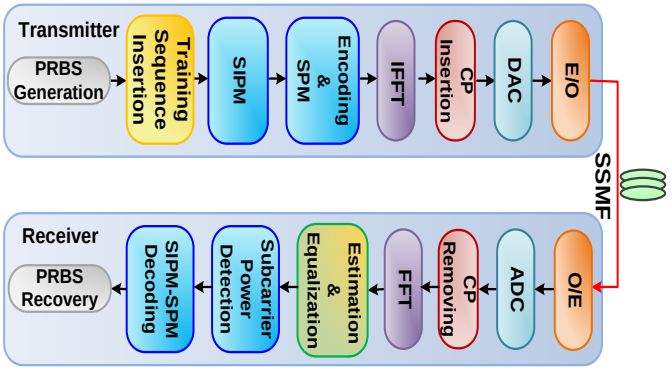

Fig.2. Schematic illustration of the SIPM-OOFDM-SPM transceiver architecture and the considered IMDD PON system.

By making use of the above-discussed SIPM-OOFDM-SPM operating principle, the relevant transceiver DSP architecture can be produced, which is schematically shown in Fig.2. Due to the DSP transceiver architecture similarity between SIPM-OOFDM-SPM, SIPM-OOFDM and conventional OOFDM [17], the general DSP procedures implemented in the SIPM-OOFDM-SPM transceiver are thus outlined below: the transmitter DSP functions consists of PRBS bit stream generation, periodic training sequence insertion, subcarrier power allocation and SIPM operation, QPSK- and 8-PSK-encoding and its relevant SPM operation, as well as serial-to-parallel (S/P) conversion. Following these processes, all information-bearing subcarriers are arranged to satisfy the Hermitian symmetry with respect to their conjugate counterparts to ensure the generation of real-valued OFDM symbols after performing the inverse FFT (IFFT). At the output of the IFFT, cyclic prefix addition and digital-to-analogue conversion (DAC) are also performed. The generated final electrical signal drives an ideal optical intensity modulator to perform the electrical-to-optical (E-O) conversion. The E-O conversion process produces an optical output signal, $s_o(t)$, having an amplitude waveform governed by

$$s_o(t) = \sqrt{s_e(t)} \tag{3}$$

where $s_e(t)$ is the electrical driving current of the SIPM-OOFDM-SPM signal with an optimum DC bias current being added.

A standard single-mode fibre (SSMF) simulation model based on the widely adopted split-step Fourier method is used to simulate the propagation of an optical signal over IMDD PON systems. In the SSMF simulation model, the effects of linear loss, chromatic dispersion and Kerr effect-induced dependence of refractive index on optical power are included [18].

In the receiver, the optical signal is converted to the electrical domain by a square-law photodetector subject to both shot and thermal noise. After passing through an analogue low bandpass filter and analogue-to-digital convertor (ADC), the following major receiver DSP functions are performed: synchronization, cyclic prefix removal, FFT for generating complex-valued frequency domain subcarriers, channel estimation and equalization, subcarrier power detection, subcarrier power threshold calculation, information recovery in the subcarrier index-power dimension and the conventional subcarrier-information-carrying dimension, as well as analysis of individual subcarrier BERs and overall channel BERs.

TABLE I
TRANSCEIVER AND TRANSMISSION SYSTEM PARAMETERS

Parameter	Value
Total number of IFFT/FFT points	64
Data-carrying subcarriers	31
Modulation formats	QPSK or 8-PSK +QPSK
PRBS data sequence length	500,000 bits
Cyclic prefix	25%
DAC & ADC sampling rate	12.5 GS/s
DAC & ADC bit resolution	9 bits
Clipping ratio	12 dB
Power ratio between 8-PSK and QPSK	2.75
Initial QPSK phase	34°
PIN detector sensitivity	-19 dBm*
PIN responsivity	0.8 A/W
SSMF dispersion parameter at 1550 nm	16 ps/(nm.km)
SSMF dispersion slope at 1550 nm	0.07 ps/nm/nm/km
Linear fiber attenuation	0.2 dB/km
Kerr coefficient	2.35×10^{-20} m²/W

*Corresponding to 10Gb/s non-return-to-zero data at a BER of 1.0×10^{-9}

III. TRANSCEIVER PARAMETER OPTIMIZATION

Having discussed the general SIPM-OOFDM-SPM operating principle in Section II, in this section, detailed numerical simulations are undertaken to identify optimum key transceiver design parameters. Throughout this paper, unless explicitly stated in corresponding texts, the following default transceiver parameters are taken: a PRBS stream of 500000 bits, IFFT/FFT points of 64, 25% cyclic prefix, training sequences periodically inserted at a space of 50 OFDM symbols, and DAC/ADC sampling rates of 12.5GS/s. Identical signal clipping ratios are always employed in the transmitter and the receiver. The abovementioned transceiver parameters are also listed in Table I. Moreover, to explicitly distinguish the advantages associated with the proposed technique, comparisons are always made between SIPM-OOFDM-SPM, 8-PSK/QPSK-encoded SIPM-OOFDM and 32-PSK/QPSK-encoded SIPM-OOFDM for all cases presented

in Section III and Section IV.

Fig.3 explores the optimum transceiver operation parameters closely related to two salient features of the proposed technique, i.e., subcarrier index-power modulation (SIPM) and SPM operation. As the power ratio, which is defined as the ratio of the powers between 8-PSK and QPSK in the transmitter, plays a key role in the SIPM operation, Fig. 3(a) explores its impact on the transceiver BER performance to identify its optimum value. Whilst Fig. 3(b) reveals the optimum QPSK initial phase setting with respect to 8-PSK prior to the SPM operation.

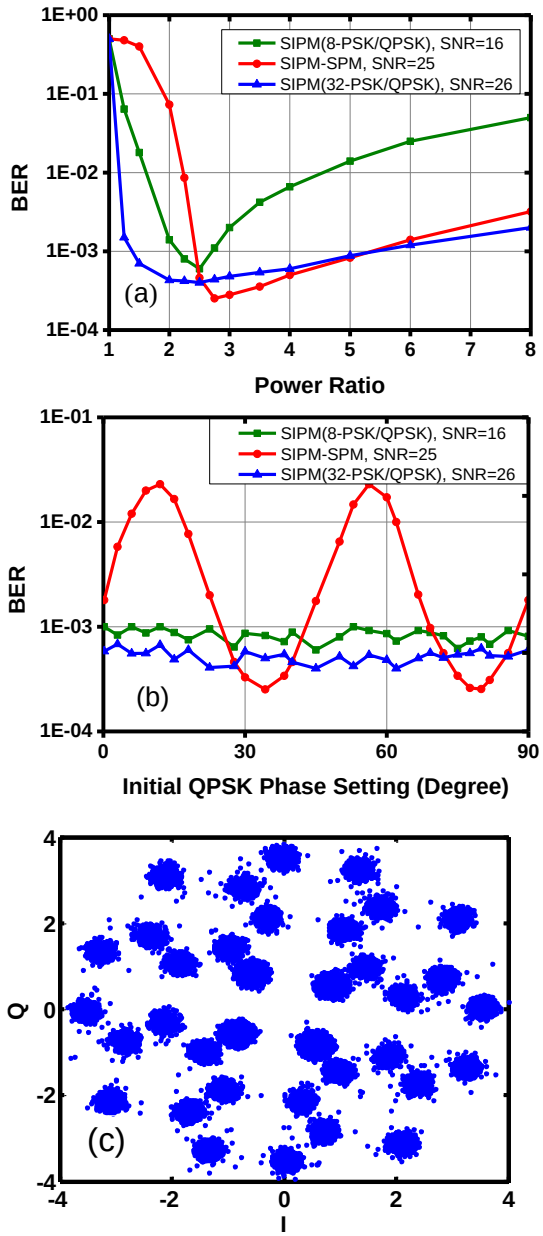

Fig.3. Optimum transceiver operation parameter identifications for different transmission techniques. (a) Optimum power ratio, (b) Optimum initial QPSK phase setting with respect to 8-PSK. (c) Overall equalized SIPM-OOFDM-SPM constellation diagram obtained at a SNR of 25dB. In calculating all these three figures, AWGN channels are considered, and the signal clipping ratio and quantization bits are fixed at 12dB and 9 bits, respectively.

In obtaining Fig.3, simple additive white Gaussian noise (AWGN) channels are considered to highlight the impact of these inherent SIPM-OOFDM-SPM features on the transceiver BER performance. The signal clipping ratio and DAC/ADC quantization bits are fixed at 12dB and 9 bits, respectively. In addition, for 8-PSK/QPSK-encoded SIPM-OOFDM, SIPM-OOFDM-SPM and 32-PSK/QPSK-encoded SIPM-OOFDM, different SNRs of 16dB, 25dB and 26dB are also chosen, respectively, as these SNRs enable these three transmission techniques to achieve BERs of $<1.0\times10^{-3}$ over the AWGN channels, as seen in Fig.6. The averaged electrical powers of these three signals remain constant.

It is shown in Fig. 3(a) that SIPM-OOFDM-SPM has an optimum power ratio of 2.75, which is similar to those corresponding to other two transmission techniques. For power ratios lower than 2.75, the BERs shoot up with decreasing power ratio, mainly resulting from the fast reduction in the minimum Euclidean distance of the SPM-generated 32-point constellation carried by the high power subcarriers; On the other hand, for power ratios larger than 2.75, the BERs grow relatively slowly with increasing power ratio, this is because the fixed electrical signal power-induced slow reduction in the minimum Euclidean distance of the 4-point QPSK constellation carried by the low power subcarriers.

It is easy to understand from Fig.1(c) that a phase rotation of QPSK with respect to 8-PSK alters the SPM-generated 32-point constellation and thus its minimum Euclidean distance. Such statement is verified in Fig.3(b), where a periodic BER developing curve occurs for SIPM-OOFDM-SPM only, and the BER curves for all other two SPM-free transmission techniques remain almost constant. In Fig. 3(b), with respect to 8-PSK, an optimum initial QPSK phase setting of 34^{o} is observed, corresponding to which the minimum Euclidean distance of the SPM-generated 32-point constellation is maximized. The observed difference of 45^{o} between two consecutive optimum QPSK phase settings is determined by the phase difference between two consecutive 8-PSK constellation points. Fig. 3(b) suggests that the SPM operation may offer a simple and effective approach of independently manipulating a feature of a signal constellation to satisfy a specific application without affecting the overall signal performance.

To gain an in-depth understanding of the aforementioned optimization processes, by making use of simulation conditions similar to those adopted in Fig. 3(a) and Fig.3(b), an overall equalized SIPM-OOFDM-SPM constellation diagram obtained at a SNR of 25dB is shown in Fig. 3(c), where the optimum power ratio and the optimum phase offset between 8-PSK and QPSK are considered.

To identify the optimum transceiver design parameters closely related to the most critical components, i.e., DACs/ADCs, Fig.4 is presented, where the impacts of clipping ratio and quantization bit on the transceiver BER performance over AWGN channels are plotted in Fig. 4(a) with fixed quantization bits of 9, and Fig. 4(b) with fixed clipping ratios of 12dB, respectively. In simulating Fig.4, use is also made of simulation parameters similar to those adopted in Fig.3. In

particular, the identified optimum power ratio of 2.75 is taken along with an optimum initial QPSK phase setting of 34°.

It can be seen in Fig. 4(a) that, for all the considered transmission techniques, their BERs reach the lowest values at clipping ratios of 12dB. For clipping ratios of <12dB, the considerable BER growth with decreasing clipping ratio is due to strong clipping-induced serious distortions to signal waveforms. Whilst for clipping ratios beyond 12dB, the increase in BER is because of the enhanced quantization noise effect associated with increased dynamic ranges. Our simulations show that, by making use of the identified optimum transceiver parameters and the default parameters listed in Table I, conventional OOFDM, SIPM-OOFDM and SIPM-OOFDM-SPM have almost identical peak-to-average power ratios (PAPRs). As a direct result, very similar optimum clipping ratios are observed in Fig. 4(a).

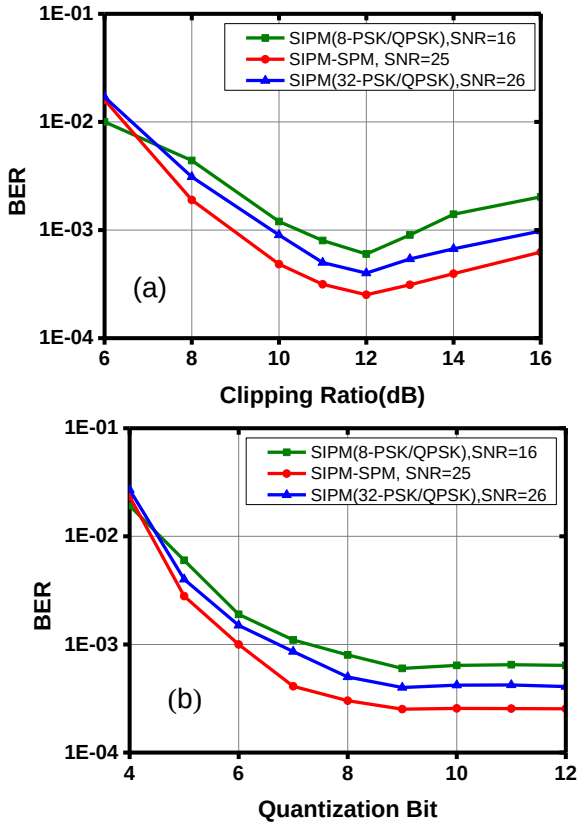

Fig.4. Overall BER performances against major DAC/ADC parameters over AWGN channels for three different transmission techniques. (a) BER versus clipping ratio. The quantization bits are fixed at 9. (b) BER versus quantization bit. The clipping ratio is taken to be 12dB.

Based on Fig. 4(a), it is easy to understand the existence of minimum quantization bits of 9 for all transmission techniques in Fig. 4(b). It is shown in Fig. 4(b) that, for low quantization bits of <9, the BER increases quickly due to the low quantization bit-induced enhancement in the quantization noise effect. Whilst for quantization bits of >9, the quantization noise effect is almost negligible, thus giving rise to almost flattened BER developing trends in Fig. 4(b). The occurrence of BER floors in Fig. 4(b) is mainly due to the use of a fixed SNR for each transmission technique considered.

TABLE II
SIGNAL BIT RATES OF DIFFERENT TECHNIQUES

Transmission Technique	Signal Bit Rate(Gb/s)
SIPM-OOFDM (8-PSK/QPSK)	20.77
SIPM-OOFDM-SPM	26.71
SIPM-OOFDM(32-PSK/QPSK)	26.71

IV. SIPM-OOFDM-SPM TRANSMISSION CHARACTERISTICS

The thrust of this section is to utilize the optimum transceiver parameters identified in Section III to explore achievable SIPM-OOFDM-SPM transmission performances over both AWGN and optical amplifier-free IMDD PON systems.

For numerically simulating the performance characteristics of these three techniques in IMDD PON systems, as listed in Table I, the following default parameters are taken: a PIN photodetector with a quantum efficiency of 0.8A/W and a receiver sensitivity of -19dBm (corresponding to a 10Gb/s non-return-to-zero data sequence at a BER of 1.0×10^{-9}), a linear fiber loss of 0.2dB/km and an optical wavelength of 1550nm. A SSMF is adopted, whose key parameters are: a chromatic dispersion parameter of 16.0ps/(km·nm), a dispersion slope of 0.07ps/nm/nm/km, an effective area of 80μm^2 and a Kerr coefficient of 2.35×10^{-20}m^2/W. All other parameters that are not explicitly mentioned above are stated in corresponding text parts.

A. Signal transmission capacity

By making use of the identified optimum transceiver design parameters and the default transceiver parameters listed in Table I, and also by taking into account 64 subcarriers per symbol, the signal transmission capacities of SIPM-OOFDM-SPM, 8-PSK/QPSK-encoded SIPM-OOFDM and 32-PSK/QPSK-encoded SIPM-OOFDM can be computed, which are summarized in Table II. Throughout this paper, raw signal transmission capacities are considered, which do not take into account the cyclic prefix effect and just include the signal transmission capacity reduction due to the addition of the training sequence. It can be seen in Table II that SIPM-OOFDM-SPM supports a signal transmission capacity of 26.71Gb/s, which exceeds 8-PSK/QPSK-encoded SIPM-OOFDM by 28.6%. Although 32-PSK/QPSK-encoded SIPM-OOFDM is capable of offering the same signal transmission capacity of 26.71Gb/s, it, however, suffers high OSNR and degraded tolerances to both chromatic dispersion and fiber nonlinearity, as analyzed below in detail.

Based on the above-discussed SIPM-OOFDM-SPM operating principle, the SIPM-OOFDM-SPM signal transmission capacity, R_b, can be expressed as:

$$R_b = \frac{f_S\left[\rho_H\left(b_H+1\right)+\rho_L\left(b_L+1\right)\right]\left(\frac{N}{2}-1\right)}{N\left(1+\alpha\right)} \qquad (4)$$

where f_s is the DAC/ADC sampling rate, ρ_H and ρ_L ($\rho_H+\rho_L=1$), are the occurrence probabilities of high and low power subcarriers within a symbol. b_H and b_L are the number of information bits carried by the high and low power subcarriers, respectively. N is the total number of subcarrier per symbol, and α is the coefficient introduced to take into account signal

transmission capacity reductions due to training sequence. Eq.(4) implies that the SIPM-OOFDM-SPM transmission capacity is subcarrier count-dependent.

The above analytical prediction is confirmed by numerically simulated results presented in Fig.5, where the signal transmission capacities of these three transmission techniques are plotted as a function of subcarrier count per symbol. In obtaining Fig.5, an AWGN channel is considered and the SNRs of three corresponding signals are fixed at 25dB. Fig.5 shows the predicted subcarrier count-dependent behaviors, which become more pronounced when the total number of subcarriers are less than 64. In addition, an almost perfect signal transmission capacity overlap between SIPM-OOFDM-SPM and 32-PSK/QPSK-encoded SIPM-OOFDM is also observed in Fig.5, indicating that, instead of SPM, SIPM is the major physical mechanism underpinning such a behavior. It should be noted that the subcarrier count-dependent signal transmission capacity is in sharp contrast to conventional OOFDM.

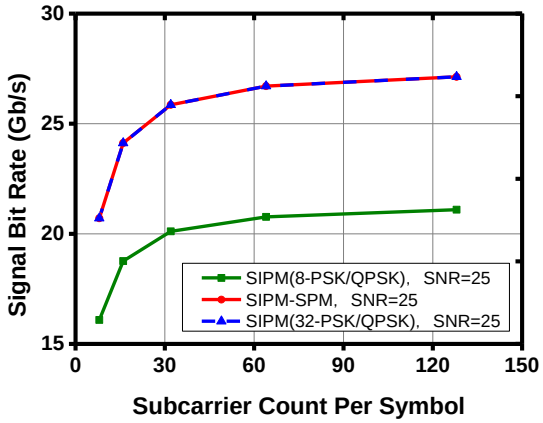

Fig.5. Subcarrier count-dependent signal transmission capacities for three transmission techniques considered. The AWGN channels are considered and the SNRs of all signals are fixed at 25dB.

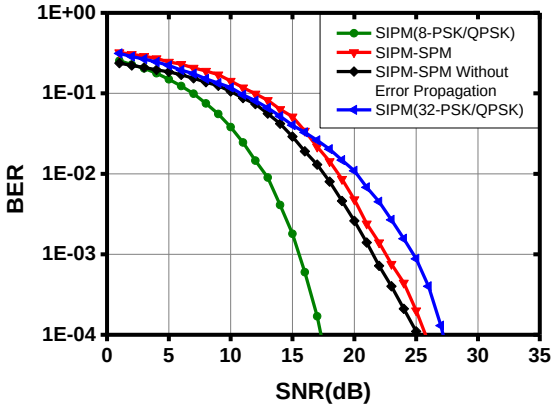

Fig.6. BER versus electrical SNR performances of three transmission techniques over AWGN channels. An error propagation-free SIPM-OOFDM-SPM BER curve is also shown.

B. BER performance over AWGN channels

The BER versus electrical SNR performances of three considered transmission techniques over AWGN channels are presented in Fig. 6. To explicitly distinguish the influence of the error propagation effect on signal SNR, an error propagation-free SIPM-OOFDM-SPM BER curve is also computed and subsequently plotted in Fig. 6 by employing an error propagation removal approach reported in [12]. By comparing the BER curves between SIPM-OOFDM-SPM, 32-PSK/QPSK-encoded SIPM-OOFDM and error propagation-free SIPM-OOFDM-SPM, it is very interesting to note that SPM gives rise to an approximately 3dB SNR gain at a BER of 1.0×10^{-3}, which is, however, offset by an proximately 1dB SNR penalty introduced by the error propagation effect, thus leading to an overall SNR gain of 2dB. The physical origin of the SNR gain is mainly due to the SPM-induced increase in the minimum Euclidean distance of the SPM-generated 32-point constellation.

In addition, the error propagation-induced 1dB SNR penalty for SIPM-OOFDM-SPM is almost identical to that corresponding to 8-PSK/QPSK-encoded SIPM-OOFDM [12], this suggests that SPM does not contribute to the error propagation effect, and that the error propagation effect is independent of signal modulation formats taken on the subcarriers. This conclusion is valuable when much more sophisticated SPM operations employing high-order signal modulation formats are applied to provide desired performances for specific application scenarios.

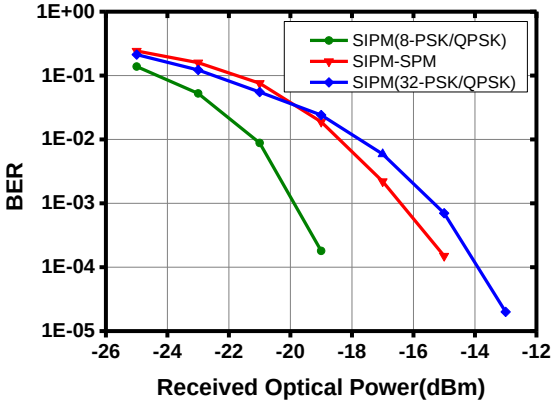

Fig.7. BER as a function of received optical power after transmitting through 25km SSMF IMDD PON systems for 26.71Gb/s SIPM-OOFDM-SPM signals, 20.77Gb/s 8-PSK/QPSK-encoded SIPM-OOFDM signals and 26.71Gb/s 32-PSK/QPSK-encoded SIPM-OOFDM signals.

C. Transmission performance over 25km IMDD PON systems

The BER versus received optical power performances of the considered three transmission techniques are given in Fig.7 after transmitting through 25km SSMF IMDD PON systems. For all the cases, the optical launch powers are taken to be 5dBm. As expected from Fig. 6, Fig.7 shows that SIPM-OOFDM-SPM can support 26.71Gb/s signal transmissions over 25km SSMF IMDD PON systems. On the contrary, when SIPM-OOFDM is applied, to achieve the same signal transmission capacity, high-order signal modulation formats such as 32-PSK/QPSK have to be adopted, which, however, cause an approximately 1dB optical power penalty at a BER of 1.0×10^{-3}, as seen in Fig.7. Such an optical power penalty agrees very well with the corresponding electrical SNR penalty observed in Fig.6. The channel fading effect associated with the considered 25km SSMF IMDD PON system is negligible, as the system frequency response roll-off effect induced by the DAC/ADC, various RF gain stages and the intensity modulator is not included. As such, numerical simulations show that the use of the well-known adaptive bit/power loading technique [17] does not considerably

enhance the SIPM-OOFDM-SPM transmission capacity. However, for IMDD PON systems suffering from the severe channel fading effect, it is envisaged that a considerable improvement in SIPM-OOFDM-SPM transmission capacity is achievable when use is made of the adaptive bit/power loading technique [16].

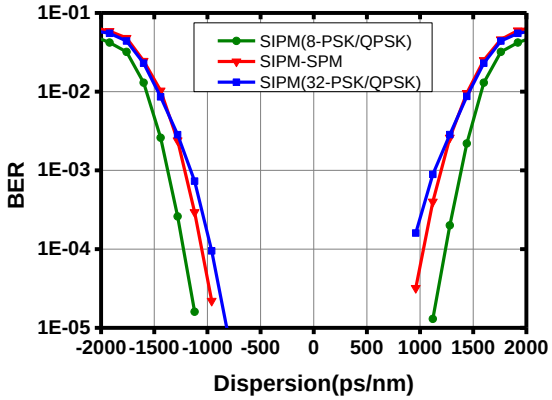

Fig.8. Performance tolerance to chromatic dispersion of IMDD PON systems for 26.71Gb/s SIPM-OOFDM-SPM signals, 20.77Gb/s 8-PSK/QPSK-encoded SIPM-OOFDM signals and 26.71Gb/s 32-PSK/QPSK-encoded SIPM-OOFDM signals.

The reduction in received optical power can be directly transferred to the optical link power budget improvement, such improvement can also be utilized to improve the SIPM-OOFDM-SPM transmission tolerance to both chromatic dispersion and fiber nonlinearity associated with the IMDD PON systems. This is numerically verified in Fig.8 and Fig.9. In Fig.8, the BERs of these three considered transmission techniques are plotted as a function of chromatic dispersion of the IMDD PON systems. In simulating this figure, various SSMF lengths ranging from 10km to 125km are taken, and the optical launch powers are fixed at 5dBm. In addition, the Kerr effect-related fiber nonlinearity and fiber linear attenuation are also disabled. The fiber dispersion parameters of -16.0ps/(km·nm) and 16.0ps/(km·nm) are used to represent the negative and positive chromatic dispersion regions, respectively.

For these three transmission techniques, the aforementioned parameters ensure chromatic dispersion-limited BER performances in both the negative and positive dispersion regions. As shown in Fig.8, in comparison with the 26.71Gb/s 32-PSK/QPSK-encoded SIPM-OOFDM signal, an increase in dispersion tolerance range of approximately 130ps/nm at a BER of 1.0×10^{-3} is feasible for the SIPM-OOFDM-SPM signal of the same signal transmission capacity.

For the 26.71Gb/s SIPM-OOFDM-SPM signal, the 20.77Gb/s 8-PSK/QPSK-encoded SIPM-OOFDM signal and the 26.71Gb/s 32-PSK/QPSK-encoded SIPM-OOFDM signal, their performance tolerances to fiber nonlinearity of the 25km SSMF IMDD PON systems are explored in Fig.9, where the BERs of these signals are plotted as a function of optical launch power, by taking into account simulation parameters identical to Fig.7. Here all the fiber linear and nonlinear effects (excluding stimulated Brillouin scattering) are present. These parameters give rise to photodetector thermal noise-limited BER performances for optical launch powers of <-10dBm, and fiber nonlinearity-limited BER performances for optical launch powers of >10dBm.

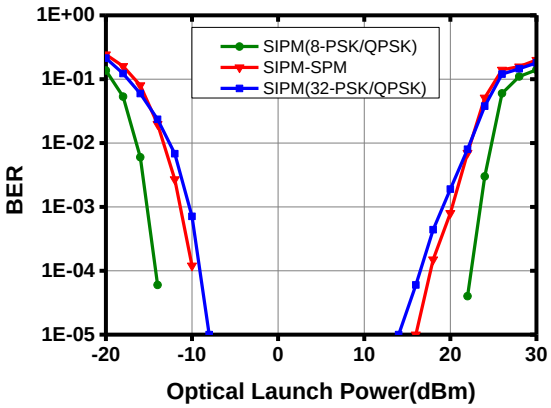

Fig.9. Performance tolerance to fibre nonlinearity of 25km SSMF IMDD PON systems for 26.71Gb/s SIPM-OOFDM-SPM signals, 20.77Gb/s 8-PSK/QPSK-encoded SIPM-OOFDM signals and 26.71Gb/s 32-PSK/QPSK-encoded SIPM-OOFDM signals.

As expected, Fig.9 shows that, compared to 32-PSK/QPSK-encoded SIPM-OOFDM, SIPM-OOFDM-SPM enhances the optical launch power dynamic range by approximately 2.2dB at a BER of 1.0×10^{-3}. The observed 2.2dB improvement in optical launch power dynamic range is a direct result of the SPM-induced reduction in minimum received optical power at a BER of 1.0×10^{-3}, as discussed in Fig.7. This indicates that SIPM-OOFDM-SPM improves system performance tolerance to fiber nonlinearity.

V. Conclusions

A novel transmission technique known as SIPM-OOFDM-SPM has been proposed and investigated, for the first time, in AWGN and 25km SSMF IMDD PON systems. Detailed numerical simulations of SIPM-OOFDM-SPM transmission characteristics over AWGN channels have been undertaken, based on which optimum SIPM-OOFDM-SPM transceiver design parameters are identified in terms of power ratio, initial QPSK phase setting, signal clipping ratio and minimum required quantization bits. By making use of the identified optimum transceiver parameters, extensive explorations have also been undertaken of the achievable SIPM-OOFDM-SPM transmission performances over 25km SSMF IMDD PON systems. It has been shown that SIPM-OOFDM-SPM supports 26.71Gb/s signal transmissions over 25km SSMF IMDD PON systems, and that a 28.6% signal transmission capacity improvement is achievable compared to the previously reported 8-PSK/QPSK-encoded SIPM-OOFDM technique. In addition, the research work has also indicated that, in comparison with the 32-PSK/QPSK-encoded SIPM-OOFDM technique capable of offering a signal transmission capacity identical to SIPM-OOFDM-SPM, the proposed technique improves the system power budget and performance tolerance to both chromatic dispersion and fiber nonlinearity.

To verify the proposed SIPM-OOFDM-SPM technique and the theoretical predictions presented in the paper, experimental

investigations are currently being undertaken in our research lab, and corresponding results will be reported elsewhere in due course.

REFERENCES

[1] J. Kani, F. Bourgart, A. Cui, A. Rafel, M. Campbell, R. Davey and S. Rodrigues, "Next-generation PON-part I: Technology roadmap and general requirements," *IEEE Commun. Magazine*, vol. 47, no. 11, pp. 43-49, Nov. 2009.

[2] E. Wong, "Next-generation broadband access networks and technologies," *J. Lightw. Technol*., vol. 30, no. 4, pp. 597-608, Feb. 2012.

[3] J. Man, S. Fu, H. Zhang, J. Gao, L. Zeng, and X. Liu, "Downstream transmission of pre-distorted 25-Gb/s faster-than-Nyquist PON with 10G-class optics achieving over 31 dB link budget without optical amplification," in *Proc. Optical Fibre Communication (OFC) Conference*, Mar. 2016, Th1I.5, pp.1-3.

[4] N. Cvijetic, "OFDM for next-generation optical access networks," *J. Lightw. Technol.*, vol.30, no.4, pp. 384-398, Feb. 2012.

[5] X. Duan, R.P. Giddings, M. Bolea, Y. Ling, B. Cao, S. Mansoor and J.M. Tang, "Real-time experimental demonstrations of software reconfigurable optical OFDM transceivers utilizing DSP-based digital orthogonal filters for SDN PONs" *Optics Express,* vol.22, no.16, pp.19674-19685, Aug. 2014.

[6] M. Seimetz, High-order Modulation for Optical Fiber Transmission, In Optical Sciences. Heidelberg, Germany: Springer, 2009, vol. 143.

[7] P. J. Winzer and R. J. Essiambre, "Advanced modulation formats for high-capacity optical transport networks," *J. Lightw. Technol*., vol. 24, no. 12, pp. 4711-4728, Dec. 2006.

[8] R. Abu-alhiga and H. Haas, ''Subcarrier-index modulation OFDM,'' in *Proc. IEEE Int. Sym. Personal, Indoor Mobile Radio Commun*., Sep. 2009, pp. 177-181.

[9] D. Tsonev, S. Sinanovic, and H. Haas, "Enhanced subcarrier index modulation (SIM) OFDM," in *Proc. IEEE GLOBECOM Workshops*, Dec. 2011, pp. 728-732.

[10] E. Başar, Ü. Aygölü, E. Panayırcı, and H. V. Poor, ''Orthogonal frequency division multiplexing with index modulation,'' *IEEE Trans. on Signal Processing*, vol. 61, no.22, pp.5536-5549, Nov. 2013.

[11] F. Halabi, L. Chen, S. Parre, S. Barthomeuf, R. P. Giddings, C. Aupetit-Berthelemot and J. M. Tang, "Subcarrier index-power modulated optical OFDM(SIPM-OOFDM) for IMDD PON systems,'' in *Proc. Optical Fibre Communication (OFC) Conference*, Mar. 2016, Th3C.1, pp.1-3.

[12] F. Halabi, L. Chen, S. Parre, S. Barthomeuf, R. P. Giddings, C. Aupetit-Berthelemot, A. Hamié and J. M. Tang, "Subcarrier index-power modulated optical OFDM and its performance in IMDD PON systems,''*J. Lightw. Technol*., vol. 34, no.9, pp.2228-2234, May 2016.

[13] Y. Saito, Y. Kishiyama, A. Benjebbour, T. Nakamura, A. Li and K. Higuchi, "Non-orthogonal multiple access (NOMA) for cellular future radio access," in *Proc. IEEE Vehicular Technology Conference (VTC Spring)*, Jun. 2013, pp. 1-5.

[14] Z. Ding, Z. Yang, P. Fan and H. V. Poor, ''On the performance of non-orthogonal multiple access in 5G systems with randomly deployed users,'' *IEEE Signal Processing Letters*, vol. 21, no.12, pp.1501-1505, Dec. 2014.

[15] S. Timotheou and I. Krikidis, ''Fairness for non-orthogonal multiple access in 5G systems,'' *IEEE Signal Processing Letters*, vol. 22, no.10, pp.1647-1651, Oct. 2015.

[16] X. Q. Jin, J. L. Wei, R. P. Giddings, T. Quinlan, S. Walker and J. M. Tang, "Experimental demonstrations and extensive comparisons of end-to-end real-time optical OFDM transceivers with adaptive bit and/or power loading," IEEE Photon. J., vol.3, no.3, pp.500-511, June 2011.

[17] R. Giddings, ''Real-time digital signal processing for OFDM-base future optical access networks,'' J. Lightw. Technol., vol. 32, no.4, pp.553-570, Feb. 2014.

[18] G. P. Agrawal, Fibre-Optic Communication Systems, 2nd ed. Hoboken, NJ, USA: Wiley, 1997.